A. L. L. Murari[1] , H. G. Tabares[1], G. A. L. Vargas[1], E. A. Belati[1] , V. A. de Sousa[2], M. B. C. Salles[3] and A. J. Sguarezi Filho[1]

UFABC (1), UFSCar (2), USP - PEA (3)

Study of Transmission System with Wind Power Control and Optimal Reactive Power Flow

Abstract. *This paper presents a methodology of controlling the power injected into system by wind generators and the use of Optimal Reactive Power Flow (ORPF). The methodology used two stages: in the first one scheme for Doubly-Fed Induction Generator (DFIG) is realized to control the active and reactive powers, in the second stage, the ORPF based in the Modified Barrier Lagrangian Function approach (MBLF) is used to optimize reactive power dispatch aiming to minimize active power losses system. Case studies on the modified IEEE 14 bus "modified" clearly shows the benefits of using the associated generator control whit ORPF.*

Streszczenie. *Artykuł przedstawia metodologię sterowania dołączaniem energii z elektrowni wiatorwych do systemu energetycznego oraz użytkowania algorytmu RRPF – Optimal Reactive Energy Flow. W pierwszym etapie analizowano sterowanie generatorem typu DFIG w celu kontroli mocy biernej i czynnej, w drugim etapie wykorzystano metodę MBLF (Modified Barrier Lagrangian Function) do optymalizowania mocy biernekj w systemie.* ***Analiza systemu energetycznego ze sterowaną mocą elektrowni wiatrowych i optymalnym przesyłem mocy***

Keywords: Optimal Reactive Power Flow; Wind Power Control; Transmission System
Słowa kluczowe: optymalizacja mocy biernej, sterowanie mocą, system energetyczny.

doi:10.12915/pe.2014.07.17

1. Introduction

Year after year technology and society´s “eco-thoughts” evolved together, bringing out new concepts such as sustainability and green corporative compliances. The human development and the access of technology makes energy demands continuously grows while natural sources like: oil, coal and gas becomes low . World consumption of electrical energy will increase by 84% between 2008-2035 [1], while in Brazil the increase will be 4.6% between 2010-2020 [2]. At this scenario smart grids involving hybrids power generation systems into distributed power generation created a new era for energy distribution. These systems are usually composed by parallel connection of photovoltaic solar panels and wind generators. Although the most advantageous solution for standalone use is the wind generator [3], where the energy produced by wind is considered technically usable when at a height of 50m the winds have speeds of at least 7 m/s [4].

The doubly fed induction generator (DFIG) is a generator type commonly employed in this type of application [5]. The techniques for independent control of active and reactive powers of DFIG are traditionally performed by the technique of the stator flux orientation or grid voltage by controlling the rotor currents [6]. Initially the aero generators were designed to operate with unity power factor, however, some studies [7] [8] presents techniques for controls reactive power of DFIG, that enable the operation of the generator supplying reactive to the network. With the reactive power control of the DFIG, the optimal reactive power injection can be evaluated respecting the DFIG´s constraints for wind speed, specified load/generation and constraints of the power system. This optimal can be evaluated via optimal reactive power flow (ORPF), which promotes management efficiencies, as improvements in voltage profile and lower losses in active power. The ORPF is a non convex static nonlinear programming problem; it is one of the most powerful tools to analyses static systems of electrical energy. The ORPF used has the objective of minimizing a function and, at the same time, of satisfying a set of physical and operational constraints in power systems, e.g. reactive power injection constraint. As a solution, it provides the optimal operation point for the electrical network for a given load and generation configuration of the system satisfying all system constraints. It was proposed by Carpentier in the early 60's based on the economic dispatch problem [9]. Since then, many papers have been written in an attempt to solve the problem [10-13].

This work considers the reactive power injection capacity of a wind farm using DFIG to optimize the active power losses in a power system. In this way is proposed to use an ORPF for a system with DFIG. The DFIG´s power control is achieved by using stator flux orientation and proportional plus integral controller. The dynamic machine model was used to obtain the steady state output of active and reactive power to be supplied to the ORFP algorithm. The ORPF algorithm uses the Modified Barrier Lagrangian Function (MBLF) [14] in the process solution. In the section 3 the ORPF problem and MBLF is displayed. Thus, the contribution of this paper is the analyzes of the benefits of the reactive power injection, by an wind farm with reactive power control, to the power system provided by optimal reactive power injecting control performed via ORPF.

This paper is organized as follows: Section 2 presents the machine model and rotor current vector control. Section 3 describes the ORPF approach used. The simulation results, which demonstrate the effectiveness of the analyses, are shown and discussed in Section 4. Finally, in Section 5 some concluding remarks are made.

2. Wind Generator Control

2.1. Rotor side converter:

For decoupled control of active and reactive power, it is necessary the induction machine dynamics model, also assuming stator flux, where the flux vector is aligned with the direct axis $\psi_s = \psi_{sd} = \left|\vec{\psi}_{sdq}\right|$, and $v_s = v_{sq} = \left|\vec{v}_{sdq}\right|$ [5].

The DFIG power control is achieved by rotor current control. Hence the independent stator active P and reactive Q power control. In this case, P and Q are computed by each individual rotor current. The active and reactive power are done by [5],

$$P = -\frac{3}{2} v_s \frac{L_M}{L_s} i_{rq} \tag{1}$$

$$Q = \frac{3}{2} v_s \left(\frac{\psi_s}{L_s} - \frac{L_M}{L_s} i_{rd} \right) \tag{2}$$

Thus, it is possible to control de active and reactive power of DFIG by the rotor current control. Proportional plus integral controllers (PI) can used for this objective as shonw in Fig. 1.

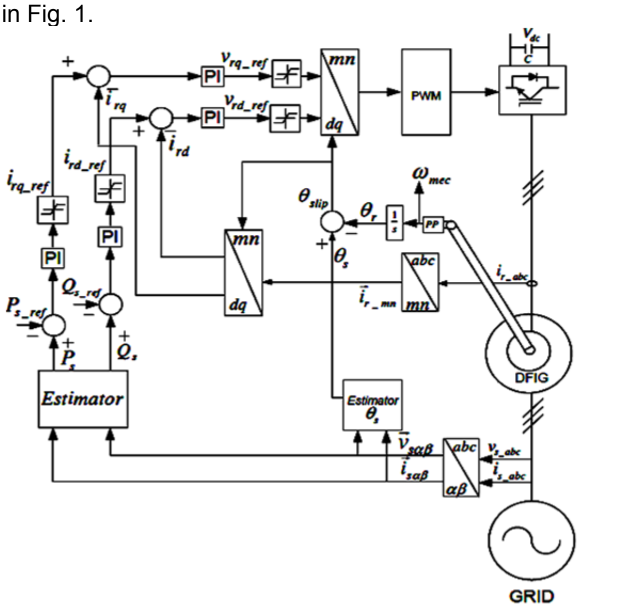

Fig. 1. Power control system for DFIG, using PIs controllers.

2.2 Grid side converter:

The grid side converter (GSC) controls the DC link voltage of the back-to-back converter, also controls the current flows through the converter and the electrical grid by using voltage [15]. Thus, it is possible to control power sent to the grid independently from the relationship:

$$P_g = \frac{3}{2} v_{gd} i_{gd} \tag{3}$$

$$Q_g = \frac{3}{2} v_{gd} i_{gq} \tag{4}$$

PI controllers can be used in this control application again. A detailed explanation can be seen in [5,15].

The Figure 2 shows the GSC control strategy.

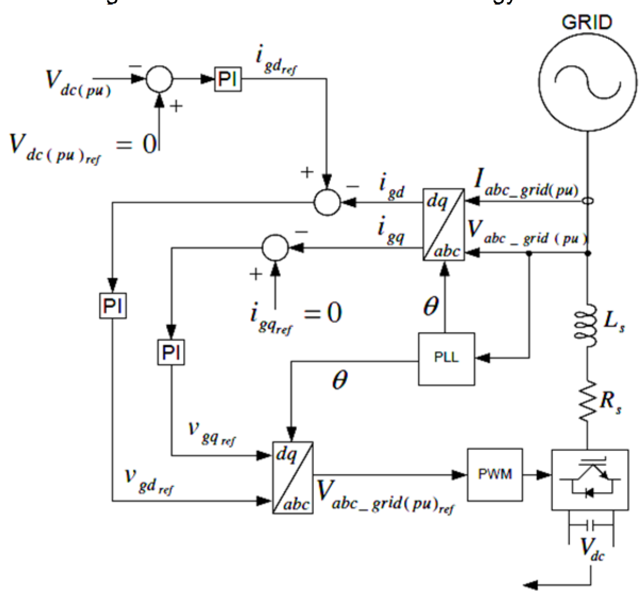

Fig. 2. GSC control block diagram.

3. Optimal Reactive Power Flow

3.1 The Problem

The ORPF problem can be described by Eq. (5).

$$\begin{aligned} & min\ f(\boldsymbol{x}) \\ & s.t \quad g_i(\boldsymbol{x})=0, \qquad i=1,...,m \\ & \qquad h_j^{min} \le h_j(\boldsymbol{x}) \le h_j^{max}, \qquad j=1,...,r \\ & \qquad \boldsymbol{x}^{min} \le \boldsymbol{x} \le \boldsymbol{x}^{max} \end{aligned} \tag{5}$$

where $\boldsymbol{x} \in R^n$ is the control and state variable vector representing voltage magnitudes ($\boldsymbol{V}$), voltage angles ($\boldsymbol{\theta}$) and tap-changing transformer ($\boldsymbol{t}$).

3.1.2 Objective Function

In this paper, the power transmission loss function $f(\boldsymbol{x})$ is set as the objective function. The power transmission loss can be expressed by Eq. (6).

$$f(\boldsymbol{x}) = \sum_{k=1}^{NL} g_{km}\left(V_k^2 + V_m^2 - 2V_k V_m \cos\theta_{km}\right) \tag{6}$$

where V_k is the voltage magnitude at bus k, g_{km} is the conductance of line k-m, θ_{km} is the difference in voltage angle between the k and m bus and NL is the total number of transmission lines.

3.1.3 Equality Constraints

The equality constraints $\boldsymbol{g}(\boldsymbol{x}) \in R^m$ represent the power flow equations that provide a means for calculating the power balance that exists in the network during steady-state operation to active and reactive power and are represented by Eq. (7) and Eq. (8) respectively.

$$\begin{aligned} P_k(\boldsymbol{x}) = P_{Gk} - P_{Lk} = \\ V_k \sum_{m \in k} V_m\left(G_{km}\cos\theta_{km} + B_{km}\sin\theta_{km}\right) \end{aligned} \tag{7}$$

$$\begin{aligned} Q_k(\boldsymbol{x}) = Q_{Gk} - Q_{Lk} + Q_k^{sh} = \\ V_k \sum_{m \in k} V_m\left(G_{km}\sin\theta_{km} - B_{km}\cos\theta_{km}\right) \end{aligned} \tag{8}$$

where P_k and Q_k are, respectively, the active and reactive power injections at bus; P_{Gk} and Q_{Gk} are, respectively, the scheduled active and reactive power generations at bus k; P_{Lk} and Q_{Lk} are, respectively, the active and reactive power loads at bus k; Q_k^{sh} is the component reactive power injection due to the shunt element at bus k; G_{km} is the real part of the element in the bus admittance matrix Y_{BUS} corresponding to the *kth* row and *mth* column, B_{km} is the imaginary part of the element in the Y_{BUS} corresponding to the *kth* row and *mth* column.

3.1.4. Inequality Constraints

All variables have upper and lower bounds that must be satisfied in the optimal solution. In this paper the functional constraints $h(\boldsymbol{x}) \in R^r$, with lower bound h_j^{min} and upper bound h_j^{max} represent the limits of reactive power injections and the inequality $\boldsymbol{x}^{min} \le \boldsymbol{x} \le \boldsymbol{x}^{max}$ the variables bounded $\boldsymbol{V}$ and $\boldsymbol{\theta}$, presented as:

$$Q_k^{min} \le Q_k(\boldsymbol{x}) \le Q_k^{max}, \tag{9}$$

$$V_k^{min} \le V_k \le V_k^{max}, \tag{10}$$

$$\theta_k^{min} \le \theta_k \le \theta_k^{max}, \tag{11}$$

where Q_k^{min} and Q_k^{max} are, respectively, the lower and upper bounds of Q_k, V_k^{min} and V_k^{max} are, respectively, the lower and upper bounds of V_k and θ_k^{min} and θ_k^{max} are, respectively, the lower and upper bounds of θ_k. These inequality constraints must be satisfied in the optimal solution.

This is a typical nonlinear and no convex problem. The ORPF used employs the formulation presented in Sousa et al. [14]. This formulation considers the application of logarithmic barrier method to voltage magnitude, voltage angles , tap-changing transformer variables and augmented Lagrangian method to other constraints. In this work wind turbines are treated as reactive control buses.

3.2 Modified Barrier Lagrangian Function Method

In this work, the MBLF method is used to solve the ORPF problem, Eq (5), which can be represented by Eq. (12).

$$\begin{aligned} &\text{Minimize} \quad f(\boldsymbol{x}) \\ &\text{subject to} \quad \boldsymbol{g(x)} = 0 \\ &\qquad \boldsymbol{h}^{min} \le \boldsymbol{h(x)} \le \boldsymbol{h}^{max} \end{aligned} \tag{12}$$

In this method, the bounded constraints are transformed into two inequalities and slack variables are introduced, transforming these inequalities into equalities.

$$\begin{aligned} &\text{Minimize} \quad f(\boldsymbol{x}) \\ &\text{subject to} \quad \boldsymbol{g(x)} = 0 \\ &\qquad \boldsymbol{h(x)} + \boldsymbol{s_1} = \overline{\boldsymbol{h}} \\ &\qquad \boldsymbol{h(x)} - \boldsymbol{s_2} = \underline{\boldsymbol{h}} \\ &\qquad \boldsymbol{s_1} \ge 0 \\ &\qquad \boldsymbol{s_2} \ge 0 \end{aligned} \tag{13}$$

where the slack vectors $\boldsymbol{S_1} \in R^r$ and $\boldsymbol{S_2} \in R^r$.

The slack variables of problem (13) are relaxed and treated by the Modified Barrier Functions. The non-negative conditions of problem (13) are relaxed by the barrier parameter.

$$\begin{aligned} &\text{Minimize} \quad f(\boldsymbol{x}) \\ &\text{subject to} \quad \boldsymbol{g(x)} = 0 \\ &\qquad \boldsymbol{h(x)} + \boldsymbol{s_1} = \boldsymbol{h}^{max} \\ &\qquad \boldsymbol{h(x)} - \boldsymbol{s_2} = \boldsymbol{h}^{min} \\ &\qquad \boldsymbol{s_1} \ge -\mu \\ &\qquad \boldsymbol{s_2} \ge -\mu \end{aligned} \tag{14}$$

where μ >0 is the barrier parameter. This represents an expansion of the feasible region of the original problem.

The Modified Barrier Function (MBF) $[\ln(\mu^{-1}\boldsymbol{s}+1)]$, proposed by [16], is used to transform problem (14) into the following modified problem.

$$\begin{aligned} &\text{Minimize} \quad f(\boldsymbol{x}) \\ &\text{subject to} \quad \boldsymbol{g(x)} = 0 \\ &\qquad \boldsymbol{h(x)} + \boldsymbol{s_1} = \boldsymbol{h}^{mas} \\ &\qquad \boldsymbol{h(x)} - \boldsymbol{s_2} = \boldsymbol{h}^{min} \\ &\qquad \mu \ln(\mu^{-1}\boldsymbol{s_1} + 1) \ge 0 \\ &\qquad \mu \ln(\mu^{-1}\boldsymbol{s_2} + 1) \ge 0 \end{aligned} \tag{15}$$

The following Lagrangian function is associated to problem (15). It is called the modified barrier Lagrangian function.

$$\begin{aligned} L = {}& f(\boldsymbol{x}) - \mu\sum_{i=1}^{p} \boldsymbol{u_{1i}} \ln(\mu^{-1}\boldsymbol{s_{1i}} + 1) - \mu\sum_{j=1}^{p} \boldsymbol{u_{2j}} \ln(\mu^{-1}\boldsymbol{s_{2j}} + 1) - \\ & \boldsymbol{\lambda}^T \boldsymbol{g(x)} - \boldsymbol{\pi_1}(\boldsymbol{h(x)} + \boldsymbol{s_1} - \overline{\boldsymbol{h}}) - \boldsymbol{\pi_2}(\boldsymbol{h(x)} - \boldsymbol{s_2} - \underline{\boldsymbol{h}}) \end{aligned} \tag{16}$$

where $\boldsymbol{u_1} \in R^r$, $\boldsymbol{u_2} \in R^r$, $\boldsymbol{\lambda} \in R^m, \boldsymbol{\pi_1} \in R^r$ and $\boldsymbol{\pi_2} \in R^r$ are the vectors of the Lagrange multipliers.

The first-order necessary conditions are applied to Eq (16), generating nonlinear system equations. Then Newton's method is applied to the nonlinear system equations to find the search direction vector $\Delta\boldsymbol{d}$ resulting in linear system equations represented by Eq (17).

$$\boldsymbol{W}\Delta\boldsymbol{d} = -\nabla_d L \tag{17}$$

The direction vector is given by $\Delta\boldsymbol{d}^T = (\Delta\boldsymbol{x}, \Delta\boldsymbol{s}_1, \Delta\boldsymbol{s}_2, \Delta\boldsymbol{\lambda}, \Delta\boldsymbol{\pi}_1, \Delta\boldsymbol{\pi}_2)$. The Hessian matrix, **W** is given by

$$\boldsymbol{W} = \begin{pmatrix} \nabla^2_{xx}L & 0 & 0 & -\boldsymbol{J}(x)^T & -\boldsymbol{J}_1(x)^T & -\boldsymbol{J}_1(x)^T \\ 0 & \mu^{-1}\boldsymbol{S}_1 & 0 & 0 & \boldsymbol{I} & 0 \\ 0 & 0 & \mu^{-1}\boldsymbol{S}_2 & 0 & 0 & -\boldsymbol{I} \\ -\boldsymbol{J}(x) & 0 & 0 & 0 & 0 & 0 \\ -\boldsymbol{J}_1(x) & \boldsymbol{I} & 0 & 0 & 0 & 0 \\ -\boldsymbol{J}_1(x) & 0 & -\boldsymbol{I} & 0 & 0 & 0 \end{pmatrix} \text{ with:}$$

$$\nabla^2_{xx}L = \nabla^2_{xx}f(\boldsymbol{x}) - \sum_{i=1}^{m}\lambda_i \nabla^2_{xx}\boldsymbol{g}_i(\boldsymbol{x}) - \sum_{j=1}^{p}\pi_{1j}\nabla^2_{xx}\boldsymbol{h}_j(\boldsymbol{x}) - \sum_{j=1}^{p}\pi_{2j}\nabla^2_{xx}\boldsymbol{h}_j(\boldsymbol{x}),$$

and the sub matrixes $\boldsymbol{S}_1$ and $\boldsymbol{S}_2$ given by

$$\boldsymbol{S}_1 = \begin{pmatrix} \frac{\boldsymbol{u}_{11}}{(\mu^{-1}\boldsymbol{s}_{11}+1)^2} & & 0 \\ & \ddots & \\ 0 & & \frac{\boldsymbol{u}_{1p}}{(\mu^{-1}\boldsymbol{s}_{1p}+1)^2} \end{pmatrix} \text{ and } \boldsymbol{S}_2 = \begin{pmatrix} \frac{\boldsymbol{u}_{21}}{(\mu^{-1}\boldsymbol{s}_{21}+1)^2} & & 0 \\ & \ddots & \\ 0 & & \frac{\boldsymbol{u}_{2p}}{(\mu^{-1}\boldsymbol{s}_{2p}+1)^2} \end{pmatrix}.$$

The Hessian matrix is sparse and symmetric and its structure is constant through iterations.

Using the search directions obtained from (17), the vectors of variables $\boldsymbol{x}$, $\boldsymbol{s}$, λ and π are updated as follows:

$$\begin{aligned} \boldsymbol{x}^{k+1} &= \boldsymbol{x}^k + \alpha_p\Delta\boldsymbol{x}^k & \boldsymbol{\lambda}^{k+1} &= \boldsymbol{\lambda}^k + \alpha_d\Delta\boldsymbol{\lambda}^k \\ \boldsymbol{s}_1^{k+1} &= \boldsymbol{s}_1^k + \alpha_p\Delta\boldsymbol{s}_1^k & \boldsymbol{\pi}_1^{k+1} &= \boldsymbol{\pi}_1^k + \alpha_d\Delta\boldsymbol{\pi}_1^k \\ \boldsymbol{s}_2^{k+1} &= \boldsymbol{s}_2^k + \alpha_p\Delta\boldsymbol{s}_2^k & \boldsymbol{\pi}_2^{k+1} &= \boldsymbol{\pi}_2^k + \alpha_d\Delta\boldsymbol{\pi}_2^k \end{aligned} \tag{18}$$

where α_p and α_d are the scalar step sizes used to update the primal and dual variables, respectively. The step sizes are calculated according to [10].

$$\alpha_p = \min\{\ -\frac{\boldsymbol{s}}{\Delta\boldsymbol{s}} : \Delta\boldsymbol{s} < 0 \text{ and } \boldsymbol{s} > 0,\ 1\ \}$$

$$\alpha_d = min\{\ -\frac{\boldsymbol{\pi_1}}{\Delta\boldsymbol{\pi_1}} : \Delta\boldsymbol{\pi_1} < 0 \ and\ \boldsymbol{\pi_1} > 0, \frac{\boldsymbol{\pi_2}}{\Delta\boldsymbol{\pi_2}} : \Delta\boldsymbol{\pi_2} < 0 \ and\ \boldsymbol{\pi_2} > 0,\ 1\ \}$$

The barrier parameter is smoothly decreased according to [17], as follows:

$$\mu^{k+1} = \mu^k\left(1 - \left(\sigma/\sqrt{2r}\right)\right) \tag{19}$$

where:

$$\sigma = max\left(1/\left(\mu^{-1}\boldsymbol{s}_j + 1\right)\right), \qquad j = 1,\dots,2r \qquad \text{for } \boldsymbol{s}_j > 0$$

The Lagrange multiplier vector, $\boldsymbol{u}$, is updated according to rule [16], which has a very low computational complexity, as follows:

(20) $\boldsymbol{u}^{k+1} = \boldsymbol{u}^{k}\,\mu^{k+1} / \left(\boldsymbol{s}^{k+1} + \mu^{k+1}\right)$

3.2.1 Simplified algorithm

Initialization Step

- Given problem (12), construct the MBLF (16);
- Let k = 0;
- Choose initial values for the problem variables:
  $\boldsymbol{d}^{k} = (\boldsymbol{x}^{k}, \boldsymbol{s}^{k}, \lambda^{k}, \pi^{k})$, $\boldsymbol{u}^{k} > 0$ and $\mu^{k} > 0$.
  x: can be the same as the initial values for a power flow, λ=0, $\pi_1 \geq 0$ and $\pi_2 \leq 0$ or any other reasonable guess.
- Go to **Main Steps**.

Main Steps

1. Evaluate ∇L as a function of ***d***.
2. Evaluate matrix $\boldsymbol{W}$ as a function of $\boldsymbol{d}$ and solve the system (17).
3. Compute the step length α_p and α_d. Update $\boldsymbol{d}$ by $\Delta \boldsymbol{d}$ and the step lengths.
4. If $\boldsymbol{d}^{k+1}$ satisfies the convergence criteria, then **STOP**. If not, then set k=k+1, update μ and the Lagrange multipliers, ***u***, using (19) and (20) respectively, and then return to Step **1**;

In the solution the Karush-Kuhn-Tucker conditions, $\boldsymbol{s} \geq 0$, $\pi_1 \geq 0$ and $\pi_2 \leq 0$, must be satisfied.

In [14] is shown that computationally this formulation is more attractive.

4. Simulation Results

The reactive power control strategy was simulated using MATLAB/SimPowerSystems package. The DFIG parameters are shown in Appendix (Tables A.1 – A.3). Figure B.1 shows the schematic of the implemented system. The inverter was modeled as controlled voltage source. It was simulated the wind energy system making the FP = 0.95 and several wind operation as shown in Table A.2 due to the fact in this work the maximum power factor is 0.95. The reactive power Q for each wind speed (more than 9m/s) can be adjusted from FP=1 till FP=0.95. The simulations results of the reactive power control made in steady state are presented in Table A.2. These results will be used by the ORPF algorithms

The analysis of a power system using the ORPF presented in section 3 with DFIGs forming a wind farm. The ORPF was implemented in FORTRAN using double-precision arithmetic. The computational work was performed on an Intel Core i5 CPU 2.5 GHz microprocessor. The studies were carried out on the modified IEEE 14 bus systems. The systems data are shown in Appendix (Tables B.1 - B.2) and main characteristics of the studied systems are summarized in the Table 1. For each test the solution was obtained with a precision of 10^{-5} pu for the power balance equations. The lower and upper voltage limits considered in the studies were 0.9 and 1.1 pu and the upper and lower voltage angle were 90° and -90°.

4.1. Validation of ORPF

The performance of the ORPF can be seen in the following comparative test in which system losses and voltage magnitude to modified IEEE 14 bus systems were compared with the Power Flow (PF) solution by Newton's Method [18]. The Figure 3 shows two voltage magnitude curves for the system using the algorithm ORPF and PF for wind speed of 14 m/s according to Table A.1. The active power losses obtained by PF totaled 7.241 and by ORPF 5.472 MW having a gain of 24.43%. The ORPF optimized the reactive power injection making the system more efficient. The liquid reactive power injection obtained via ORPF and PF was 86.599 and 146.637 Mvar respectively. In the analysis with PF was not considered the reactive power control.

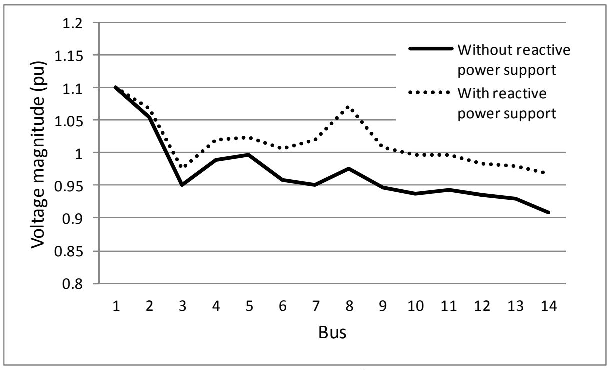

Fig. 3. Voltage magnitude to the modified IEEE 14 bus systems using the algorithms ORPF and PF.

4.2. System performance considering the DFIG

Considering the wind farm connected at bus 8 was carried out simulations for the wind conditions of 6 m/s to 14 m/s considering the data generator according to the Table A.1 for all wind speed.

Figure 4 shows in a clear way that reactive power injection contributes to improving voltage profile. From 9 m/s the generator provides reactive power. From this speed, the voltage profile improves resulting in an active power losses reduction.

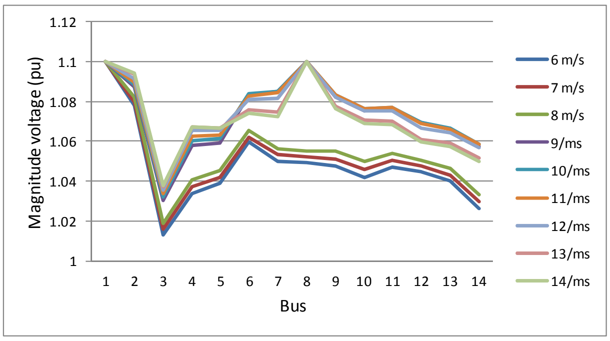

Fig. 4. Magnitude voltage to the modified IEEE 14 bus systems in relation to wind speed.

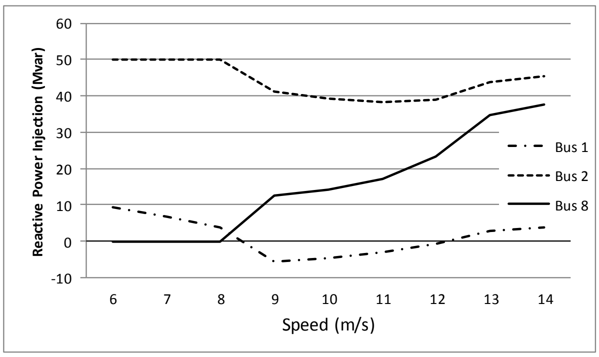

Fig. 5. Reactive power injection in the modified IEEE 14 bus systems in relation to wind speed.

The optimal reactive power injection in the system is illustrated in Figure 5. The wind farm (bus 8) presents a great contribution in the reactive power injection from 9 m/s. The bus 2 generated maxima reactive power, 50 Mvar, until 9 m/s. From this speed, the bus 8 start reactive power injection causing a decrease in the reactive power generation of the bus 2. The slack bus contributed with the reactive power balance.

The Figure 6 shows the optimal active power injection in the system. The wind farm (bus 8) injected active power in accordance with Table A.2. The bus 2 remained constant in 18.3 MW the active injection. The slack bus contributed with the active power balance.

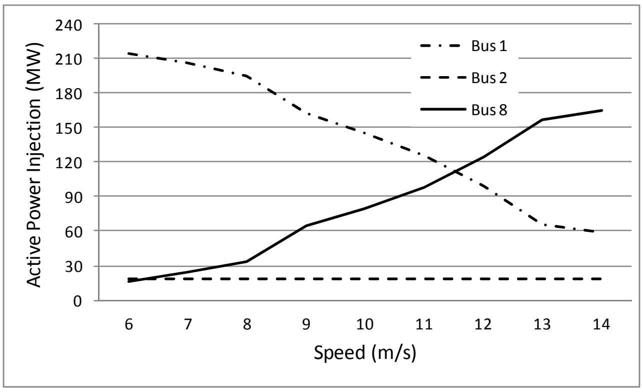

Fig. 6. Active power injection in the modified IEEE 14 bus systems in relation to wind speed.

Figure 7 illustrate the active power losses in relation to wind speed range. It shows that from speed of 13 m/s the active losses began to increase. This is due to location of the wind farm and amount of active power generated. In this situation we need to evaluate the cost of MWh to each generation. Considering that the wind generation has a low cost per MWh, this situation for system operation may be viable, even causing an increase in active power losses.

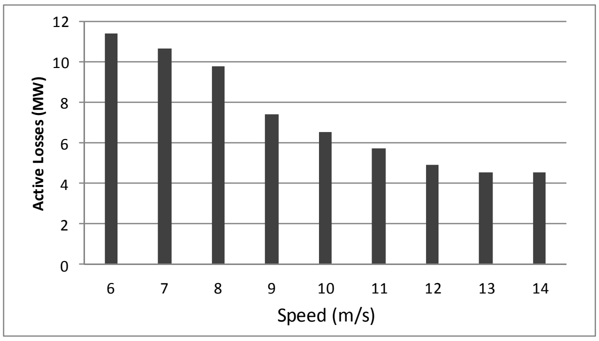

Fig. 7. Active power losses to the modified IEEE 14 bus systems in relation to wind speed.

5. Conclusions

This paper presented an approach to optimal operation of power system with reactive power control in wind turbines. In this work is used a reactive power control for DFIG-based wind turbine using stator field orientation for high control performance. The steady state simulations results are used in ORPF algorithms. An ORPF based in the Modified Barrier Lagrangian Function approach to optimize reactive power dispatch aiming to minimize active power losses system was utilized. The ORPF was able to optimize the reactive power dispatch of the system considering the operational constraints. In the tests performed with the modified IEEE 14 bus system was observed a better voltage profile and power loss which shows the importance of injecting reactive power provided from wind generators. Therefore it is evident the benefits of using wind generators with reactive power control for optimize the system.

Appendix

Table 1 - Summary of the main characteristics of the modified IEEE 14 bus system.

Buses	lines	Generation buses	Load buses	DFIG buses
14	20	2	11	1

A. Wind farm electrical systems parameters:

Table A.1 – Doubly-fed induction generator characteristic.

R_1 (pu)	0.01
L_1 (pu)	0.1
R_2 (pu)	0.01
L_2 (pu)	0.08
M_m (pu)	3
H (s)	0.5
Number of Pole	4

Table A.2 - DFIG reactive power capability.

Wind (m/s)	P (MW)	Q (Mvar)	S (MVA)	FP
6	16.3	0	16.3	1
7	23.75	0	23.75	1
8	33.85	0	33.85	1
9	64.36	21.33	67.85	0.95
10	80	26.34	84.22	0.95
11	98.55	32.5	103.77	0.95
12	124.24	40.93	130.80	0.95
13	157.32	51.76	165.61	0.95
14	164.64	54.11	173.30	0.95
The reactive power Q for each wind speed (more than 9m/s) can be adjusted from FP=1 so Q = 0 Mvar till FP=0.95 lead.				

Table A.3 - Turbine characteristic.

Min. Rotor Speed - variable speed (rpm)	9
Nom. Rotor Speed – variable speed (rpm)	14
Rotor diameter (m)	75
Area covered by rotor (m^2)	4418
Nom. Power (MW)	2
Nom. Wind Speed – variable speed (rpm)	14
Gear box ratio - variable speed	1:100
Inertia constant (s)	2.5
Shaft stiffness – fixed speed (pu/ el rad)	0.3

B. Modified IEEE 14 bus system:

Table B.1 - Data line.

from	to	r (pu)	x (pu)	b_{sh} (pu)
1	2	1.94	5.92	5.28
1	5	5.4	22.3	5.28
2	3	4.7	19.8	4.38
2	4	5.81	17.63	3.74
2	5	5.7	17.39	3.40
3	4	6.7	17.1	3.46
4	5	1.34	4.21	1.28
4	7	0.01	20.91	0
4	9	0.01	55.62	0
5	6	0.01	25.2	0
6	11	9.5	19.89	0
6	12	12.29	25.58	0
6	13	6.62	13.03	0
7	8	0.01	17.62	0
7	9	0.01	11.00	0
9	10	3.18	8.45	0
9	14	12.71	27.04	0
10	11	8.2	19.21	0
12	13	22.09	19.99	0
13	14	17.09	34.80	0

Table B.2 - Data buses with reactive control.

bus	Q (Mvar)	Q_{min} (Mvar)	Q_{max} (Mvar)
1	0	-200	200
2	12.7	-40	50
8	shown in Table A.1		

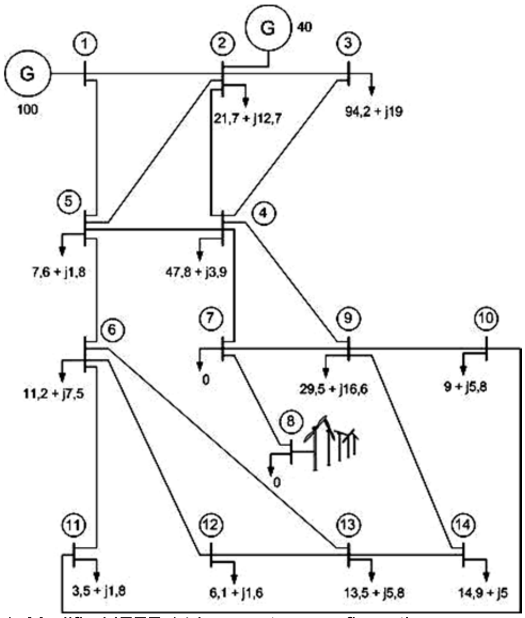

Fig. B.1. Modified IEEE 14 bus system configuration.

REFERENCES

[1] IEO2011. (International Energy Outlook 2011), accessed in 20/05/2013, avaliable at: http://www.eia.gov/forecasts/ieo/pdf/0484(2011).pdf

[2] M. Tolmasquim. (2011, 20/03). Destaques do Novo Plano Decenal de Expansão de Energia 2019 – PDE 2019.

[3] W. D. Kellogg, M. H. Nehrir, G. Venkataramanan, and V. Greez, Generating Unit Sizing and Cost Analysis for Stand-alone Wind, Photovoltaic and Hybrid Wind/PV Systems, IEEE Trans. Energy Conversion, Vol. 13, No. 1, pp. 70-75, March 1998.

[4] ANEEL. (14/05/2013). Energia Eólica. Available at: http://www.aneel.gov.br/aplicacoes/atlas/pdf/06-Energia_Eolica(3).pdf

[5] G. Abad, J. Lopez, M. A. Rodriguez, L. Marroyo and G. Iwanski, Doubly fed induction machine. IEEE Press, Ed. Wiley, 2011.

[6] X. Zheng and D. Guo, Study and Connection of DFIG to Grid Based on Double-vector PWM, 2010, Internacional Conference on Electrical and Control Engineering.

[7] Lund T, Sørensen P, Eek J. Reactive power capability of a wind turbine with doubly fed induction generator. Wind Energy. 2007;10:379-94.

[8] Engelhardt S, Erlich I, Feltes C, Kretschmann J, Shewarega F. Reactive Power Capability of Wind Turbines Based on Doubly Fed Induction Generators. IEEE Trans. on Energy Conv. 2011;26:364-72.

[9] Carpentier J. Contribution à l'étude du dispatching économique. Bulletin de la Societe Francaise des Electrciens. 1962:431- 47.

[10] Granville S. Optimal reactive dispatch through interior point methods. IEEE Trans. on Power Syst. 1994;9:136-46.

[11] Torres GL, Quintana VH. An interior-point method for nonlinear optimal power flow using voltage rectangular coordinates. IEEE Trans. on Power Syst. 1998;13:1211-8.

[12] Capitanescu F, Glavic M, Ernst D, Wehenkel L. Interior-point based algorithms for the solution of optimal power flow problems. Electr. Power Syst. Res. 2007;77:508-17.

[13] Baptista EC, Belati EA, da Costa GRM. Logarithmic barrier-augmented Lagrangian function to the optimal power flow problem. Int. J. Electr. Power Energ Syst. 2005;27:528-32.

[14] de Sousa VA, Baptista EC, da Costa GRM. Optimal reactive power flow via the modified barrier Lagrangian function approach. Electr. Power Syst. Res. 2012;84:159-64.

[15] A. Yazdani, R. Iravani. Voltage-Sourced Converters in Power Systems. A John Wiley and Sons. 2010.

[16] Polyak R. Modified barrier functions (theory and methods). Math. Program. 1992;54:177-222.

[17] Melman A. and Polyak RA. The Newton Modified Barrier Method for QP Problems, Annals of Operations Research, vol. 54, pp. 465–519, 1996.

[18] Tinney WF, Hart CE. Power Flow Solution by Newton's Method. IEEE Trans. on Power Appar. and Syst. 1967;PAS-86:1449-60.

The authors thank the Conselho Nacional de Desenvolvimento Científico e Tecnológico (CNPq) and Fundação de Amparo à Pesquisa do Estado de São Paulo (FAPESP) for financial support.

Authors:
A. L. L. Murari[1], H. G. Tabares[1], G. A. L. Vargas[1], E. A. Belati[1], V. A. de Sousa[2], M. B. C. Salles[3] and A. J. Sguarezi Filho[1]
UFABC (1), UFSCar (2), USP - PEA (3)

Corresponding uthor:
Prof. Dr. Alfeu J. Sguarezi Filho
Eng. de Instrumentação, Automação e Robótica - CECS - UFABC
Coordenador da Pós-Graduação em Eng. Elétrica da UFABC
alfeu.sguarezi@ufabc.edu.br